Formation of low-dimensional close-packed arrays of nanoparticles in a dewetting water layer

Leonid V. Govor,[1,*] Günter Reiter,[2] Gottfried H. Bauer,[1] and Jürgen Parisi[1]
[1]*Institute of Physics, University of Oldenburg, D-26111 Oldenburg, Germany*
[2]*Institut de Chimie des Surfaces et Interfaces, CNRS, 68057 Mulhouse Cedex, France*
(Received 28 May 2007; published 29 October 2007)

We report on self-assembly of $CoPt_3$ particles (diameter 6 nm) into low-dimensional close-packed arrays. This was achieved on substrates coated with a nitrocellulose (*NC*) thin layer by spreading of a hexane solution containing $CoPt_3$ particles, hexadecylamine, and water. In a first step, the solution film transforms into a bilayer containing a hexane layer located onto a water film. The hexane layer dewets the water layer and the latter dewets the *NC* covered substrate. Dewetting of the water layer leads to the formation of water droplets. Finally, the particles follow the motion of the contact line of the dewetting water layer and thus assemble into close-packed arrays at the periphery of the water droplets.

DOI: 10.1103/PhysRevE.76.041609 PACS number(s): 68.08.Bc, 81.07.−b, 81.16.Dn, 68.15.+e

I. INTRODUCTION

A self-assembled ordering of nanoparticles into low-dimensional structures is one of the most promising basic approaches to produce materials with new properties. During the past few years, the electronic properties of individual particles [1] as well as those of two- and three-dimensional arrays have been extensively studied [2]. Recently, the electronic transport through quasi-one-dimensional arrays of nanoparticles (containing four chains of particles; particle diameter 5.5 nm) was experimentally investigated [3]. So far, no experimental studies are available on truly one-dimensional arrays of particles (containing only one or two chains).

The ordering of nanoparticles to regular structures is reported in several papers. Ohara and Gelbart [4] describe ringlike structures with a diameter of 0.1–1 μm which were formed during the drying process and resulted from holes nucleating in the wetting thin liquid films that contain the nanometer-sized metal particles. Shafi *et al.* [5] have observed that nanoparticles can combine to the well-known structure of the "Olympic Rings" (intersection of rings, ring diameter 0.6–5 μm). The mechanism of ring building was explained in terms of the formation of holes in an evaporating thin film and interparticle dipolar forces. Maillard *et al.* [6] found out that the formation of ringlike structures of nanoparticles is related to Benard-Marangoni instabilities in the deposited liquid films. Tripp *et al.* [7] have shown that nanoparticles can self-assemble in similar ringlike structures as a consequence of the following processes: dipole-directed self-assembly (typically 5–12 particles, ring diameter 50–100 nm) and evaporation-driven hole formation in viscous wetting layers (ring diameter ranging from 0.5 to 10 μm). Wyrwa *et al.* [8] have described the one-dimensional arrangements of metal nanoparticles formed by self-assembly processes at the phase boundary between water and dichloromethane.

We have recently presented an experimental study of the formation of self-assembled ringlike structures of nanoparticles (diameter 6 nm) formed in an evaporating thin film [9,10]. This was achieved on a water surface by spreading a binary mixture composed of two solutions: nitrocellulose dissolved in amyl acetate and $CoPt_3$ particles stabilized by hexadecylamine (*HDA*) dissolved in hexane. The self-assembly process of the particles into micrometer-sized rings results from phase separation in a thin film of the mixed solutions, leading to a bilayer, and subsequent decomposition during solvent evaporation of the top hexadecylamine-rich layer into droplets. Finally, the evaporation of the remaining solvent from these droplets gives rise to a retraction of their contact line, and particles located at the contact line follow its motion and subsequently self-assemble along this line. We found that phase separation and ordering of nanoparticles into a ring were extremely sensitive to composition variations of the binary mixture.

In the present work, we have simplified the method described above [9,10]. We show that arrays containing one, two, three, or four parallel chains of nanoparticles can be formed as a consequence of dewetting of a thin water film on a solid substrate: nanoparticles located on the solid substrate follow the motion of the contact line (i.e., the interface between air, water, and substrate) and self-assemble along the latter.

II. EXPERIMENT

In the present experiments, hexane solutions with volume concentration 1.0×10^{-5}% and 1.3×10^{-5}% of $CoPt_3$ particles (diameter 6 nm, stabilized with *HDA* [11]) were used. Additionally, *HDA* with a concentration 1.0×10^{-3}% and water with a concentration 1.0×10^{-2}% were added to the solution. According to the specification provided by the producer (AppliChem GmbH), hexane itself contains a maximum 5×10^{-3}% of water and 5×10^{-4}% of nonvolatile matter. The comparatively high amount of water in the solution serves for ordering the nanoparticles into rings via formation of water droplets after hexane evaporation where the additional *HDA* covers the surfaces of water droplets. Consequently we are able to observe the position of the particle rings by an optical light microscope after water evaporation and to place the particle chains between two electrodes for electronic

*leonid.govor@uni-oldenburg.de

transport analysis. In other words, the additional *HDA* plays the role of tracers for the nanoparticle rings. Thin films were prepared at ambient conditions by spreading of the solution on (a) Si substrate covered with nitrocellulose (*NC*) film (thickness 100 nm); (b) transmission electron microscopy (TEM) grids covered with a *NC* film (thickness 100 nm). We found that the patterns formed on both substrates were similar.

A drop (3 μl) of the solution was cast onto a horizontal planar substrate. The deposition radius d_{s0} of the resulting solution layer spread out on the substrate amounted to about 3.5 mm, i.e., the total thickness of the layer can be estimated to about 78 μm. The radius $d_{s0}=3.5$ mm of the spread solution layer remained constant for a time span of about 17 s and then decreased quickly to the center of the spreading area. The total time span between the casting of the solution and its full drying amounted to about 20 s. In the course of hexane evaporation, the solution layer transforms into a bilayer containing a hexane layer at the solution-air interface and a water layer at the solution-substrate interface. The retraction of the hexane layer on the surface of the water layer opens the latter for a contact to air. The water layer will be unstable and decomposes into droplets. The nanoparticles located inside the solution arrange at the edge of the water droplets. Note that the time span necessary for dewetting and the total evaporation of the hexane dropletlike layer amounts to about 3 s, whereas the water droplets can be observed during a few minutes (without *HDA*). This time increases to a few days, if the solution contains *HDA*.

We want to emphasize here only a few special features observed in the present experiment: (a) similar droplet structures were formed in a closed desiccator in the presence of hygroscopic P_2O_5 powder. This excluded the presence of water in air. Thus, the cooling of the substrate by hexane evaporation and possible condensation of water at ambient conditions did not play a significant role; (b) dewetting of the thin water layer always started at the periphery of the spread film area and proceeded radially toward the center of the film; (c) the solubility of water in hexane at 20 °C is 4.27×10^{-2} mol % and that of hexane in water is 2.91×10^{-4} mol % [12]. In our experiment, we have used hexane containing either 0.01% or 0.005 vol % of water. Phase separation in the cast solution films appears in both cases. We found that the structure of the water droplets did not significantly depend on the presence or absence of *HDA* in the solution. From this we conclude that, for *HDA* concentrations up to 0.001%, the process of phase separation of water in hexane only weakly depends on *HDA*.

The temporal development of the drying process of the solution layer onto the *NC*/Si substrate was accompanied by a digital camera Nikon Coolpix 995 on an optical light microscope (magnification ×200) recording 30 frames per second. After evaporation of hexane and drying, the topography of the films located on *NC*/Si substrates and on *NC*/TEM grids was analyzed by atomic force microscopy (AFM, Dimension 3100, Digital Instruments). The arrangement of the $CoPt_3$ particles has been studied by TEM (model Zeiss EM 902) using the films located on *NC*/TEM grids.

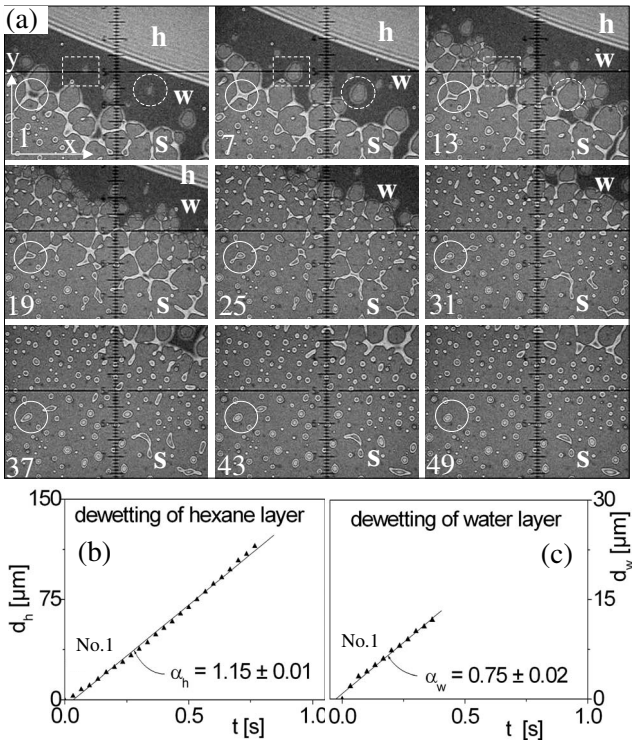

FIG. 1. (a) Typical optical micrographs for the retraction of the phase separated layers of hexane (denoted as *h*) and water (denoted as *w*) on the *NC*/Si substrate (denoted as *s*) appearing in the range $d_{s0}>d_{s1}$. The length of the smallest division (*y* direction) amounts to 5 μm. (b) Time dependence of the dewetted distance for the hexane layer (d_h) on the surface of the water layer along the *y* direction indicated in (a). (c) Time dependence of the dewetted distance for the water layer (d_w) on the surface of the *NC* layer for a hole (1) indicated by the dotted box in (a). The value of α_w for a hole (2) indicated by the dotted circle in (a) is similar to that shown for a hole (1).

III. EXPERIMENTAL RESULTS

A typical spatial and temporal evolution of the fluid solution film during its dewetting as a function of time is shown in Figs. 1–3 for three characteristic regions taken from three different samples out of a total of nine studies. For a better understanding of these figures, we denote the corresponding displacement positions of the dewetted layer edge as d_{s1} for sample 1 (Fig. 1), d_{s2} for sample 2 (Fig. 2), and d_{s3} for sample 3 (Fig. 3). Before the dewetting process has started, the radius of the initially spread area of the solution layer was $d_{s0}\approx3.5$ mm for all samples. Considering the motion of the dewetted layer edge along the radius from point $d_{s0}\approx3.5$ mm to point $d_{s0}=0$ (center of spreading area), Figs. 1–3 describe the fragments of the edge positions which can be ordered as $d_{s0}>d_{s1}>d_{s2}>d_{s3}>0$. From the total of 70 images recorded at a time interval of 33 ms, a selection of nine images are shown in each of Figs. 1–3 (number of the image is indicated in the lower left-hand corner). That means, the time span between the micrographs 1 and 7, between 7 and 13, etc., amounts to 0.2 s.

Figure 1(a) presents a fraction of the dewetting process evolved in the range $d_{s0}>d_{s1}$, i.e., where dewetting begins

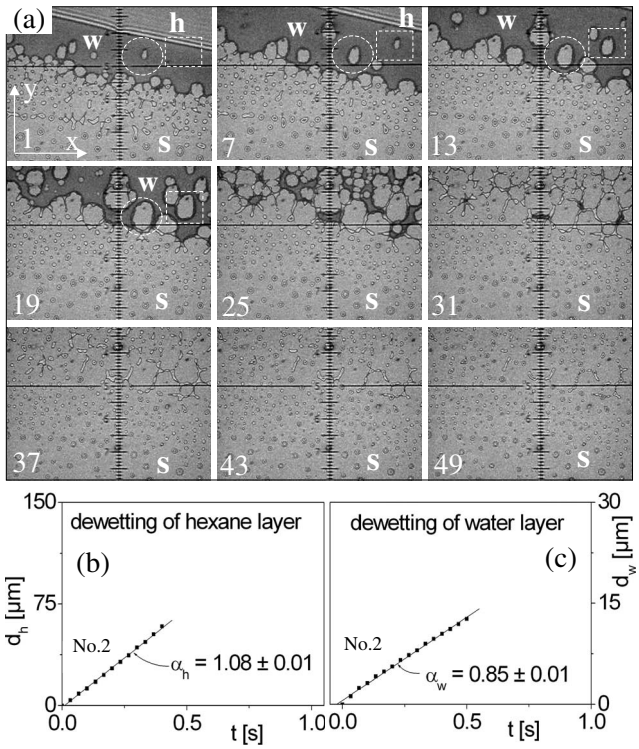

FIG. 2. (a) Typical optical micrographs for the retraction of the phase separated layers of hexane (denoted as h) and water (denoted as w) on the *NC*/Si substrate (denoted as s) appearing in the range $d_{s1} > d_{s2}$. (b) Time dependence of the dewetted distance for the hexane layer (d_h) on the surface of the water layer along the y direction indicated in (a). (c) Time dependence of the dewetted distance for the water layer (d_w) on the surface of the *NC* layer for a hole (1) indicated by the dotted box in (a). The value of α_w for a hole (2) indicated by the dotted circle in (a) is similar to that shown for a hole (1).

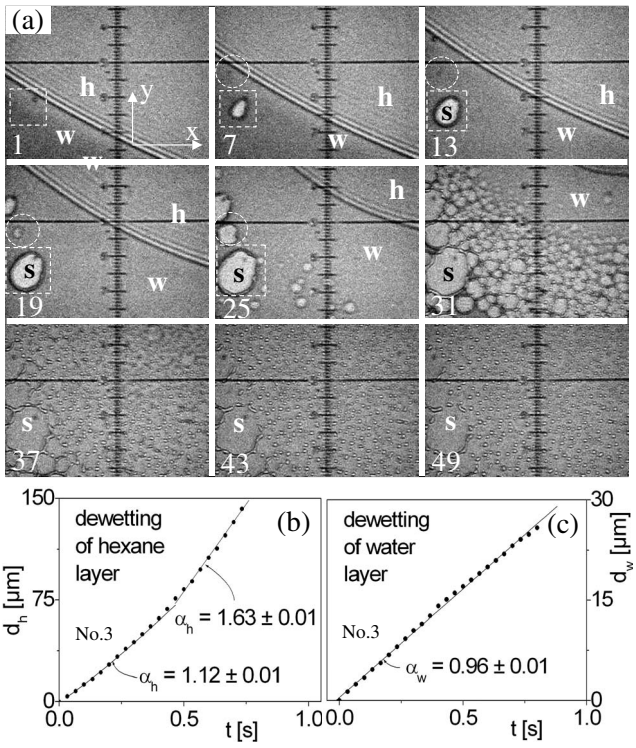

FIG. 3. (a) Typical optical micrographs for the retraction of the phase separated layers of hexane (denoted as h) and water (denoted as w) on the *NC*/Si substrate (denoted as s) appearing in the range $d_{s2} > d_{s3}$. (b) Time dependence of the dewetted distance for the hexane layer (d_h) on the surface of the water layer along the y direction indicated in (a). (c) Time dependence of the dewetted distance for the water layer (d_w) on the surface of the *NC* layer for a hole (1) indicated by the dotted box in (a). The value of α_w for a hole (2) indicated by the dotted circle in (a) is similar to that shown for a hole (1).

(sample 1). It can be clearly seen that the dewetting system consists of two layers: the top hexane layer (h) dewets on the surface of the lower water layer (w), and that dewets on the surface of the *NC*/Si substrate (s). During the dewetting process, the hexane layer turns out as the continuous film, while the water layer deforms at the beginning into the cellular structure that decomposes then into droplets. The dewetted distance of the hexane layer edge (d_h) is measured as function of time t_i. Here, $t_i = i \times 33$ ms, where $i = 1, 2, 3, \ldots$ correlates with the number of the subsequent images. The position of the contact line at $t_i = t_1$ has been defined as the starting point. The resulting experimental dependence $d_h(t)$ illustrated in Fig. 1(b) can be described as $d_h(t) = P_h t^{\alpha_h}$ with $\alpha_h = 1.15 \pm 0.01$. P_h is a time-independent prefactor. The temporal evolution of the dewetting water layer (d_w) was determined via measurement of the diameter D_w of the holes increasing with time [indicated by the dotted box and circle in Fig. 1(a)]. The dependence of d_w as a function of time t_i can be formulated as $d_w(t) = D_w(t_i)/2$ with $D_w(t_i)$ being the hole diameters at time t_i. The resulting dependence illustrated in Fig. 1(c) can be described as $d_w(t) = P_w t^{\alpha_w}$ with $\alpha_w = 0.75 \pm 0.02$. P_w is again a time-independent prefactor. The displacement position of the dewetted edges of hexane and water layers were measured within an error of ±0.5 μm being typically smaller than the symbol size in Figs. 1–3.

The dewetting process evolution in the range $d_{s1} > d_{s2}$ (sample 2) is shown in Fig. 2(a). The time dependence of the dewetted distance of the hexane layer can be described as $d_h(t) = P_h t^{\alpha_h}$ with $\alpha_h = 1.08 \pm 0.01$ [Fig. 2(b)]. The corresponding dependence of the dewetted water layer has been reproduced as $d_w(t) = P_w t^{\alpha_w}$ with $\alpha_w = 0.85 \pm 0.01$ [Fig. 2(c)]. The time dependence of the dewetted hexane layer measured in the range $d_{s2} > d_{s3}$ (sample 3) can be described as $d_h(t) = P_h t^{\alpha_h}$ with $\alpha_h = 1.12 \pm 0.01$ increasing with time to $\alpha_h = 1.63 \pm 0.01$ [Fig. 3(b)]. The corresponding time dependence of the dewetted water layer meets $d_w(t) = P_w t^{\alpha_w}$ with $\alpha_w = 0.96 \pm 0.01$ [Fig. 3(c)]. It should be noted that the values of α_w for all investigated holes located on one sample are similar.

Comparing the results observed for samples 1, 2, and 3, it can be clearly seen that dewetting of the hexane layer on the surface of the water layer proceeds with approximately constant velocity, i.e., exponent $\alpha_h \approx 1$. On the contrary, the motion of the dewetted water layer on the surface of the *NC* layer changes with time, i.e., exponent α_w increases as the water layer edge approaches the center of the spreading area. Moreover, the diameters of the polygons building the cellular

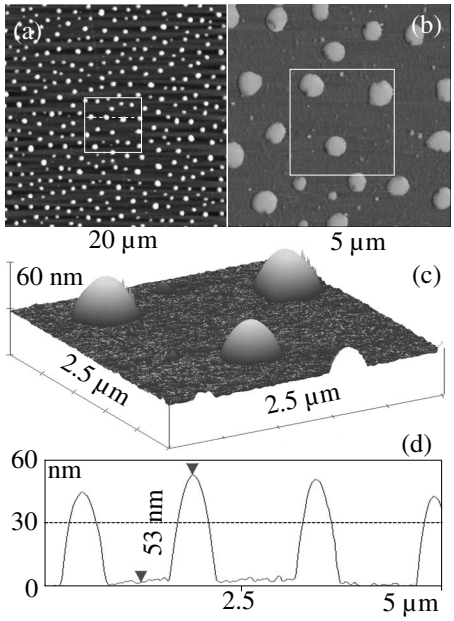

FIG. 4. Tapping-mode AFM measurements: (a) height image of water droplets located on a nitrocellulose film measured directly after spreading of the solution; (b) magnified phase image of an area indicated by the square box (solid line) in (a); (c) magnified three-dimensional image of the water droplets indicated by the box in (b); (d) profile analysis of the scan along the dotted line indicated in (a).

water structure before it decomposes into droplets are smaller in the central part of the spreading area [Fig. 3(a)] compared to those at its edge [Fig. 1(a)]. It is obvious that the decomposition of the water cellular structure into droplets develops faster in the central part of the spreading area than at its edge. These results indicate that the thickness of the water layer in the center of the spreading area is smaller than at its edge.

Figure 4 shows typical AFM images of water droplets formed in the central part of the spreading area measured directly (within about 30 min) after the spreading of the solution onto the TEM grid coated with the *NC* film. An average diameter of the droplets $D_d \approx 0.5$ μm and their average height $h_d \approx 40-50$ nm were obtained. After drying the samples for 7 weeks, the height decreased to $h_d \approx 10$ nm, without a significant change of D_d [Figs. 5(a) and 5(d)]. The remaining deposit after the complete drying of the droplets consisted of *HDA* [Figs. 5(c) and 5(d)]. That was proven via a removal of the *HDA* deposits from the dry sample by immersing the sample for a period of 5 min in hexane, which is a selective solvent for *HDA*.

Most importantly, the analysis of the droplet patterns by TEM clearly demonstrated that the $CoPt_3$ particles self-assembled into close-packed arrays located at the periphery of the droplets. For example, Fig. 5(b) illustrates the TEM image of the same droplet shown in Fig. 5(a). For a more detailed analysis of the particle array, we have attempted to take the magnified AFM and TEM images of the same fragment indicated by the square box in Figs. 5(a) and 5(b). The resulting images are shown in Figs. 6(a) and 6(b), respectively. The superposition of the contour lines taken from the

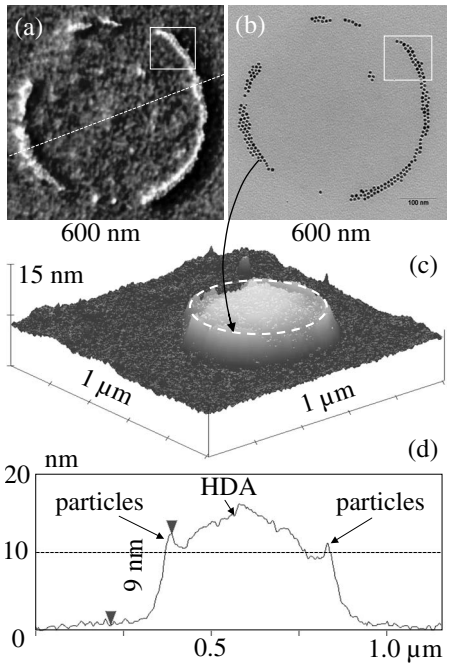

FIG. 5. (a) Tapping-mode AFM height image of a water droplet located on a *NC*/TEM grid measured after drying the samples for 7 weeks. (b) Corresponding TEM image of the same droplet shown in (a). (c) Three-dimensional image of a water droplet shown in (a). The indicated dotted ring illustrates the location of a nanoparticle ring shown in (b). (d) Profile analysis of the scan along the dotted line indicated in (a).

TEM image of the particle array shown in Fig. 6(b) with its AFM image shown in Fig. 6(a) indicates to us how the AFM images of the nanoparticle array can be analyzed correctly [Fig. 6(d)]. The latter is significant for nanoparticle arrays located on the solid substrates where TEM measurements are impossible. We found that the arrays with a different number of chains can be produced via variation of the particle con-

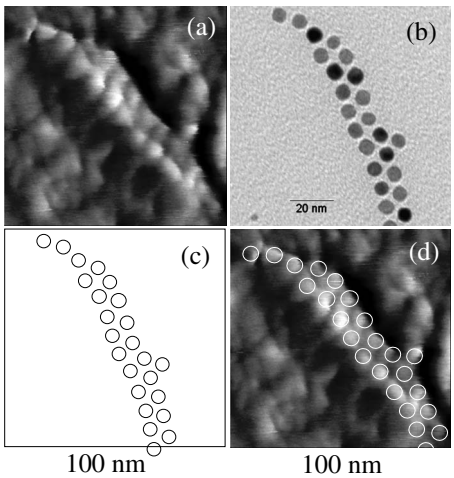

FIG. 6. (a) AFM magnified image of a $CoPt_3$ particle array indicated by the square box in Fig. 5(a). (b) TEM image of the same particle array shown in (a). (c) Contour lines taken from the particle array shown in (b). (d) Superposition of the contour lines shown in (c) with the particle array shown in (a).

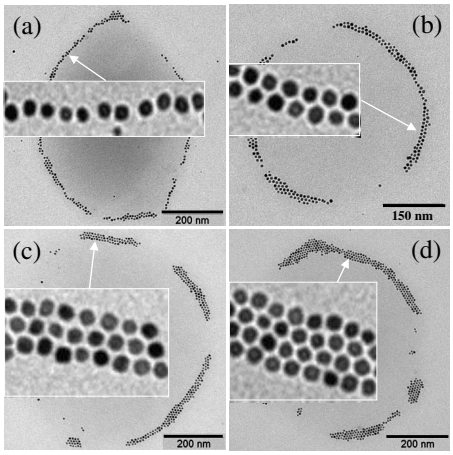

FIG. 7. TEM images of $CoPt_3$ particles ordered into rings composed of the several arrays containing mainly: (a) one chain; (b) two chains ; (c) three chains; (d) four chains. The magnified images of the indicated fragments are shown in the insets.

centration in the initial solution and via the size of the water droplets. For example, Fig. 7 displays the rings composed of several arrays containing mainly one, two, three, or four aligned chains of particles, respectively. The particle arrays shown in Fig. 7(a) are produced with a volume concentration $1.0\times10^{-5}\%$ of $CoPt_3$ particles in solution and the arrays shown in Figs. 7(b)–7(d) with a concentration $1.3\times10^{-5}\%$. We found that, for constant concentrations of water and particles in the initial solution, the average size of the particle rings (size of water droplets) and length of the ordered chains of particles (about 100 nm) were always fairly reproducible in our experiment. That means that most particle rings located on a sample were similar. For instance, on the sample illustrated in Fig. 7(a) all particle rings contained regions (about 100 nm in length) which consisted of single chains of particles. The increase of particle concentration in the initial solution leads, first, to an increase of number of such regions of single chains for each individual ring and, second, to an increase of number of the aligned chains within such regions.

IV. DISCUSSION

A. Formation of water droplet pattern

In accordance with the experimental results described above, we conclude that during hexane evaporation out of the solution film located on the substrate covered with *NC* layer the following processes occur: (a) the solution film transforms into a bilayer composed of a hexane layer on a water film; (b) the hexane layer dewets the surface of the water layer; (c) most of the particles existing in solution contact the surface of *NC* film; (d) a relevant part of *HDA* existing in solution adsorbs on the surface of the water layer, i.e., at the interface between the water and the hexane layer; (e) the water layer coated with *HDA* gets unstable and decomposes into droplets; (f) during formation of water droplets, the particles located near the droplet edge follow its motion and order along that. It should be noted that the events (a)–(f) indicated above must not be considered as a sequence, but as a list of events which appear during hexane evaporation from the solution film consisting of hexane, water, hexadecylamine, and nanoparticles. Most of these events overlap or take place simultaneously.

In more detail, the reason for phase separation of the solution layer into a bilayer is that hexane with its lower surface energy (surface tension $\gamma_h=18.4$ mN/m) wets the surface region, in order to minimize the free energy at the interface between air and solution [13]. Water with its comparatively large surface energy (surface tension $\gamma_0=72.5$ mN/m) wets the interface between the solution and the substrate. We conclude that during bilayer formation, *HDA* (surface tension $\gamma_2=25.8$ mN/m) can partially adsorb onto the surface of the *NC*/Si substrate building clusters [14], but the main part of *HDA* remains dissolved in the hexane layer. Initially, wetting of the hexane layer on water would occur in a neat bilayer, because the spreading coefficient $S_{h0}=\gamma_0-\gamma_h-\gamma_{h0}=3.0$ mN/m for pure water and hexane phases [15]. Here, $\gamma_{h0}=51.1$ mN/m [12] is the surface tension at the interface between hexane and water. However, in our resulting bilayer the top hexane layer is saturated with water and *HDA*, and the lower water layer is saturated with hexane. As a result, the value of the equilibrium spreading coefficient gets $S_{h0}\leq0$. The change from a positive initial spreading coefficient to a negative equilibrium spreading coefficient is a well-known phenomenon for short alkanes spreading on water [16,17].

We found that the experimentally observed time dependence of the dewetted distance of the hexane layer can be described as $d_h(t)\sim t^{\alpha_h}$ with $\alpha_h\approx1$ for the observed interval located between the edge and the center of the spreading area [Figs. 1(b), 2(b), and 3(b)]. Such dependence corresponds to dewetting where the driving capillary forces (uncompensated Young force) are balanced by viscous forces (forces per unit length of the three-phase contact line) [18,19]. In this case, i.e., for nonslipping films, the energy is dissipated in a small volume located at the contact line [20], and the dewetting velocity remains constant [19]. The increase of the dewetting velocity at the final stage of our experiments [exponent $\alpha_h\approx1.6$, Fig. 3(b)] might be caused by evaporation of the final amounts of hexane during the dewetting process. In general, as evaporation of hexane may affect the dynamic contact during dewetting, the total driving force may be varying in time. Thus, the interpretation of the exponent α_h may not be a trivial task.

We assume that, during dewetting and evaporation of hexane, *HDA* molecules dissolved in hexane adsorbed on the water surface. As a consequence, water droplets could be observed for a long time after the decomposition of the water layer took place. That means, the *HDA* layer, which coated the water droplets, delayed water evaporation from the droplets. Experimentally, the *HDA* layer which remained after complete water evaporation is illustrated in Fig. 5(c), where its thickness amounts to about 10 nm (measured after drying the samples for 7 weeks). For the support of the mechanism proposed above, we have cast a 3 μl droplet of hexane containing $5\times10^{-3}\%$ of water onto the *NC*/Si substrate. The micrometer-sized water droplets remaining after hexane evaporation could be observed only for a few minutes (optical light microscope with magnification $\times500$), i.e., it was

possible to immediately see how the droplet diameter decreased. A similar experiment with hexane containing $5\times10^{-3}\%$ of water and $1.0\times10^{-3}\%$ of *HDA* demonstrates that the water droplets could be observed during a few days.

The thickness of the initially formed water layer in the central part of the spreading area can be estimated from the total volume of all droplets per reference area, for example, located on the 10×10 μm^2 area as illustrated in Fig. 4(a) (excluding the volume of *HDA*, nonvolatile matter, and particles). The resulting thickness of the water layer amounts to about 4 nm, i.e., it is comparable to the particle radius. Deduced from the concentration of water in solution (0.01%), we expected on the average about 8 nm thick water layer. First, this difference can be explained due to the water evaporation which took place during the time span between spreading of the initial solution and the AFM measurements. Second, the thickness of the water layer at the edge of the spreading area is larger than in the central part (see Sec. III). In general, the stability of the water layer with a thickness of 4 nm deposited on the *NC*/Si substrate is governed by the effective molecular interactions at the interface between the *NC* layer and the surface of the water layer, for instance, by long-range van der Waals and short-range electrostatic forces [21]. The water layer located on the (*NC*) layer is unstable and starts to dewet by forming holes, because the spreading coefficient S_{01} is negative, $S_{01}=\gamma_1-\gamma_0-\gamma_{01}=-89$ mN/m [15]. Here, $\gamma_1=38$ mN/m designates the surface tension of (*NC*) (at the boundary to air); $\gamma_{01}=55$ mN/m is the interfacial tension between water and *NC*. The latter was calculated following Israelachvili [21] as $\gamma_{01}=\gamma_0+\gamma_1-2(\gamma_{0d}\gamma_1)^{0.5}$ where $\gamma_{0d}=20$ mN/m is only dispersion force contribution to the surface tension of water. Note that the value of S_{01} estimated above for pure water on *NC* film should only be considered as a qualitative indicator. When the thin water layer will be covered with *HDA*, the reductions of γ_0 and γ_{01} will have to be taken into account.

We found that the experimental time dependence of the dewetted distance of the water layer can be described as $d_w(t)\sim t^{\alpha_w}$ with α_w rising from 0.7 to 1 in the observed spatial regime located between the edge and the center of the spreading area [Figs. 1(c), 2(c), and 3(c)]. Dewetting of the water layer with $\alpha_w\approx0.7$ may reflect dewetting of a slipping film, where the capillary energy is dissipated over the whole moving part of the film proportional to the width of the rim formed by the liquid originating from the dewetted region [18,22]. The rise of α_w from 0.7 to 1 observed in our experiment could be interpreted as a transition from dewetting of slipping films to that of nonslipping films. However, as noted in the context of the exponent α_h, evaporation of water may cause a dynamic contact angle which changes in time and thus affects the exponent α_w. Systematic dewetting experiments for controlled evaporation rates would be necessary to allow an unambiguous interpretation of the dewetting exponents.

B. Formation of nanoparticle arrays

In accordance with the results described above, Fig. 8 sketches a pictorial scenario of the mechanism we propose to be responsible for the formation of the close-packed arrays of nanoparticles. Figure 8(a) schematically shows a dewetting of hexane layer on the surface of water layer. During dewetting and evaporation of hexane the nanoparticles and the most of *HDA* consisting in solution adsorb on the water surface. The diameter of the $CoPt_3$ particles coated with the *HDA* monolayer (stabilizer) amounts to 8.8 nm, i.e., it is comparable or larger than the thickness of the water layer. That means the nanoparticles can contact the *NC* film. Comparing the thickness of water droplets (40 nm) with that of the *HDA* deposits (10 nm) that were left after water evaporation [Figs. 4(d) and 5(d)], we deduce that this amount of *HDA* layer would be allowed to cover the total surface of water layer with a continuous film of about 1 nm. From the concentration of *HDA* in solution (0.001%), we expected on the average about 0.8 nm thick layer. The *HDA* molecules can adsorb on the water surface either as a monolayer with a discrete thickness of 1.4 nm (length of *HDA* molecule) or as micelles with a thickness of 2.8 nm (2 monolayers), which order into the larger clusters [14]. That means that the total water surface is only partly covered with the *HDA* clusters.

During dewetting of the water layer, the holes grow within this layer, and the removed water accumulates at the edge of the holes and builds the rims [Fig. 8(b)]. A cross section of the rim is a portion of a circle. Because the front

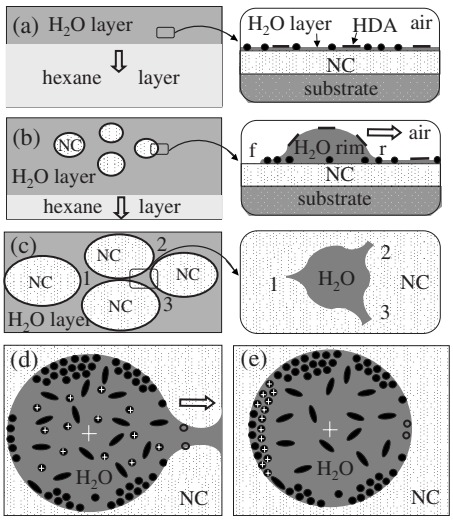

FIG. 8. Schematic illustration of the development of close-packed particle arrays via the dewetting water layer. (a) Top view of the water layer formed on the *NC*-coated substrate after dewetting and evaporation of hexane. Magnified side view of an area indicated by the square box is shown on the right-hand side. The particles are denoted as circles and the *HDA* clusters as the ellipselike plates. (b) Development of the holes appearing in the dewetting water layer. Magnified side view of the rim forming in the dewetting water layer is shown on the right-hand side; *f* and *r* denote front and rear side of the rim. (c) Formation of the cellular structure containing water ribbons. Formation of a water droplet from a fragment indicated by the square box is shown on the right-hand side. (d) Assembling of particles at the water droplet edge. The particles located in the interior of the droplet are additionally denoted with white crosses. An arrow illustrates the direction of the droplet motion before its final position. (e) Final formation of the water droplet with particles assembled at its edge.

side f of the rim is moving, the particles that are located at this contact line must follow its retraction and, consequently, assemble into the close-packed arrays along the contact line. The holes become large enough so that their rims contact each other [Fig. 8(c)]. This results in the formation of ribbons which assemble into the cellular structure. The ribbons are unstable and decompose into droplets. Most of the particles which were collected from the dewetted area assemble at the contact lines of the water droplets [Fig. 8(d)]. During the final stage of formation of the water droplet pattern, the ribbon fragments still shrink somewhat and so the particles located onto the *NC*/Si substrate in the interior of the water droplets [denoted additionally with white crosses in Fig. 8(d)] turn out to be at the droplet edge, where they assemble along their contact lines [Fig. 8(e)]. Experimentally, the shrinkage of the water droplets during their formation can be seen in Fig. 1(a), where the center of a ribbon fragment indicated by the circle in image 1 is displaced by about 3 μm and 6 μm in the x and y direction (image 49), respectively. Finally, the force governing the arrangement of particles into ordered assemblies is the capillary attraction, since the thickness of the water layer at the droplet edge is comparable to the particle diameter [23]. During the formation of water droplets, most of the particles could not move back into the droplet interior, because these capillary forces also pin the particles at the periphery of the water droplet. Note that after formation of the water droplets, most of the *HDA* clusters were located on the surface of droplets. During the final displacement of the water droplet, the positions of the *HDA* clusters on its surface change weakly [Figs. 8(d) and 8(e)]. After water evaporation out from the droplets, these clusters adsorb on the substrate, building the dropletlike deposit.

Figures 5(b) and 7 clearly demonstrate that within the interior of ringlike structures only few particles were observed. Similar images were observed for more than 100 ringlike structures. Experimentally, deduced from the concentration of particles in solution, we expected on the average about 3 nanoparticles on an area of 100×100 nm^2 of the spread film. However, this is obviously not in accordance with the experimental results shown in Figs. 5(b) and 7, where selected regions contained significantly more particles while almost no particles were found within the ringlike structures. On the one hand, the mechanism described above for the formation of close-packed arrays of particles explains the arrays observed in Figs. 5(b) and 7. On the other hand, displacement of particles from the interior of a water droplet toward its edge could be caused via the effect well known for drying liquid coffee droplets on a solid substrate, where ringlike deposits remain along the edge of the droplets [24,25]. When the contact line of a droplet is pinned, an outward flow J_f of the solvent develops, since the solvent removed via evaporation from the edge of the droplet must be replenished by J_f from the interior. This flow may drag particles to the contact line [25].

In the following, this effect will be considered as a possible mechanism for the formation of the ringlike assembly of particles observed in our study, i.e., the particles move from the center to the periphery of the water droplet during evaporation of water. We assume, that during the droplet formation, the particles could be dispersed anywhere within the droplet. Particles within the volume of the droplet will be attracted to the substrate as a consequence of gravity. The gravity force $mg=2.2\times10^{-20}$ N is larger than the buoyancy force $f_b=3.2\times10^{-21}$ N. That means, before the flow J_f can move the particles to the droplet edge, the particles tend to adsorb on the substrate, mainly on the *NC* layer and partially on the *HDA* deposit remaining on the *NC* layer after hexane evaporation. The motion of a $CoPt_3$ particle in a water droplet caused by flow J_f can be qualitatively estimated by the force equation $f_f=f_{fr}$, where $f_f=6\pi\eta r_s v$ is the flow force. Here, $\eta=0.9\times10^{-3}$ Ns/m^2 and v are viscosity and velocity of the water flow J_f, respectively. $r_s=r+\delta=4.4$ nm is the radius of the $CoPt_3$ particle coated with a *HDA* monolayer (with thickness $\delta=1.4$ nm). $f_{fr}=Kf_z$ is a lateral friction force acting on the particle moving on the substrate, where K is a dimensionless coefficient of the order unity [4] and f_z is the attraction along the vertical axis between particle and *NC* layer (or *HDA* deposit) due to dispersion forces. The interaction energy between a $CoPt_3$ particle and the *NC* layer can be described as $W(D)=-Ar/6D$ [21], and the corresponding interaction force reads $f_z=\partial W(D)/\partial D=Ar/6D^2$, where D gives the distance between the particle and the *NC* layer, and A denotes the Hamaker constant [26]. The interaction force between $CoPt_3$ particle (3) and *NC* layer (1) across the *HDA* monolayer (2) including surrounding water (0) can be approximated by [21]

$$f_z=\frac{r}{6}\left(\frac{A_{232}}{(2r)^2}-\frac{\sqrt{A_{121}A_{323}}}{(2r+\delta)^2}-\frac{\sqrt{A_{020}A_{323}}}{(2r+\delta)^2}+\frac{\sqrt{A_{020}A_{121}}}{(2r+2\delta)^2}\right). \tag{1}$$

The effective Hamaker constants A_{232}, A_{121}, A_{323}, and A_{020} have been composed by the respective Hamaker constants of each medium [27]

$$A_{232}=A_{323}=(\sqrt{A_{22}}-\sqrt{A_{33}})^2,\quad A_{121}=(\sqrt{A_{11}}-\sqrt{A_{22}})^2, \tag{2}$$

$$A_{020}=(\sqrt{A_{00}}-\sqrt{A_{22}})^2.$$

The individual Hamaker constants A_{ii} have been extracted from the individual surface tension γ_{ii} as

$$A_{ii}=24\pi\gamma_{ii}(D_o)^2, \tag{3}$$

with a cutoff intermolecular separation $D_o=0.165$ nm [21]. Equation (3) yields $A_{22}=5.3\times10^{-20}$ J for the experimentally obtained value $\gamma_2=25.8$ mN/m [9]. For the *NC* layer with $\gamma_1=38$ mN/m, the corresponding Hamaker constant amounts to $A_{11}=7.8\times10^{-20}$ J. Considering the characteristic Hamaker constant for a lot of metals [21], and accordingly for $CoPt_3$ as well, $A_{33}\approx4\times10^{-19}$ J and $A_{00}\approx1.5\times10^{-19}$ J for water with $\gamma_0=72.5$ mN/m, the effective Hamaker constants, Eq. (2), $A_{232}\approx1.6\times10^{-19}$ J, $A_{121}\approx2.4\times10^{-21}$ J, $A_{020}\approx2.5\times10^{-20}$ J could be determined. Using Eq. (1), the interaction force becomes $f_z\approx1.5\times10^{-12}$ N. Assuming $K\approx0.5$ [4], the friction force amounts to $f_{fr}\approx7.5\times10^{-13}$ N. From the balance $f_f=f_{fr}$, the velocity v of the water flow J_f necessary to move a particle located on the *NC* coated substrate from the droplet interior to its periphery would be v

$\approx 1.0\times 10^4$ μm/s. The corresponding interaction force between $CoPt_3$ particle and *HDA* covered parts of the substrate amounts to $f_z \approx 1.7\times 10^{-12}$ N and $v \approx 1.1\times 10^4$ μm/s.

It should be noted that, at present, to our knowledge, no experimental results on the flow velocity within micrometer-sized droplets of a fluid are available. For a drying water droplet with a radius of 2 mm, deposited on a solid substrate and with a pinned contact line, Deegan *et al.* [25] have measured a velocity of about 6 μm/s for polystyrene spheres with a diameter of 1 μm. The evaporation rate of water in the diffusion-limited regime was proportional to the diameter of the droplet, as a consequence of the finite probability for evaporating molecules to return to the liquid state [28]. Extrapolating this result to our case, we expect that the velocity of the flow J_f in micrometer-sized water droplets must be substantially smaller than 6 μm/s. Consequently, the value $v \approx 1.0\times 10^4$ μm/s required for transport of particles to the periphery of the droplet cannot be established.

An important question to address is the following: what if most of the particles were floating on the water surface (water-air interface) after the formation of the water droplets? In this case, the particles can move with the flow J_f from the center to the periphery of the water droplet during its evaporation. Simultaneously, the *HDA* clusters, which must be located on the surface of water droplets, must also be dragged along to the droplet edge, together with particles. If such occurs, we expect that most of the *HDA* clusters should be found together with the nanoparticles at the periphery of the droplet, i.e., the cross section of the *HDA* deposit that was left after water evaporation should have a cuplike shape. However, that is not in accordance with our experimental observation shown in Fig. 5(d) where a dropletlike profile of the *HDA* deposit is observed. Accordingly, the *HDA* clusters did not move from the center of the droplet to its periphery. We believe that the flow J_f appearing in the drying millimeter-sized water droplet located on a solid substrate [24,25] could not develop in the micrometer-sized water droplet with a thickness of only a few tens of nm. If most of the particles were left on the surface of the water droplet, one would have to anticipate that, after complete water evaporation, these particles would be spread all over the contact area of the droplets, similar to the deposit of the *HDA* clusters. This does not agree with our experimental results. That means, after formation of water droplets, most particles were preferentially located at the water-*NC* film interface. According to our results, it can be assumed that practically all particles in the ringlike structures were assembled due to the motion of the contact line of the thin water layer during its dewetting and not due to flow-induced transport to the droplet edges.

V. CONCLUSION

In summary, it has been demonstrated experimentally that during hexane evaporation from a thin film of a hexane solution containing also $CoPt_3$ particles, *HDA*, and water, the following processes occur: (a) the solution film transforms into a bilayer containing a hexane layer located on a water layer; (b) the hexane layer dewets the surface of the water layer; (c) most of the particles have contact to the substrate; (d) the main part of the *HDA* existing in solution adsorbs on the surface of the water layer, i.e., at the interface between the water and the hexane layer; (e) the water layer coated with *HDA* will be unstable and decomposes into droplets; (f) during formation of water droplets, the particles located near the droplet edge follow its motion and order.

ACKNOWLEDGMENTS

The authors would like to thank E. Shevchenko and H. Weller for the preparation of $CoPt_3$ nanoparticles, moreover, M. Burchardt for taking the atomic force microscopy pictures.

[1] J. von Delft and D. C. Ralf, Phys. Rep. **345**, 61 (2001).
[2] D. Yu, C. J. Wang, B. L. Wehrenberg, and P. Guyot-Sionnest, Phys. Rev. Lett. **92**, 216802 (2004); N. Y. Morgan, C. A. Leatherdale, M. Drndic, M. V. Jarosz, M. A. Kastner, and M. Bawendi, Phys. Rev. B **66**, 075339 (2002); R. Parthasarathy, X. M. Lin, and H. M. Jaeger, Phys. Rev. Lett. **87**, 186807 (2001).
[3] K. Elteto, X. M. Lin, and H. M. Jaeger, Phys. Rev. B **71**, 205412 (2005).
[4] P. C. Ohara and W. M. Gelbart, Langmuir **14**, 3418 (1998).
[5] K. V. P. M. Shafi, I. Felner, Y. Mastai, and A. Gedanken, J. Phys. Chem. **103**, 3358 (1999).
[6] M. Maillard, L. Motte, A. T. Ngo, and M. P. Pileni, J. Phys. Chem. **104**, 11871 (2000); M. Maillard, L. Motte, and M. P. Pileni, Adv. Mater. (Weinheim, Ger.) **13**, 200 (2001).
[7] S. L. Tripp, S. V. Pusztay, A. E. Ribbe, and A. Wei, J. Am. Chem. Soc. **124**, 7914 (2002).
[8] D. Wyrwa, N. Beyer, and G. Schmid, Nano Lett. **2**, 419 (2002).
[9] L. V. Govor, G. Reiter, J. Parisi, and G. H. Bauer, Phys. Rev. E **69**, 061609 (2004).
[10] L. V. Govor, G. Reiter, G. H. Bauer, and J. Parisi, Appl. Phys. Lett. **84**, 4774 (2004).
[11] E. Shevchenko, D. Talapin, A. Kornowski, A. Rogach, and H. Weller, J. Am. Chem. Soc. **124**, 11480 (2002).
[12] A. H. Demond and A. S. Lindner, Environ. Sci. Technol. **27**, 2318 (1993).
[13] F. Bruder and R. Brenn, Phys. Rev. Lett. **69**, 624 (1992); U. Steiner, J. Klein, and L. J. Fetters, *ibid.* **72**, 1498 (1994); W. Straub, F. Bruder, R. Brenn, G. Krausch, H. Bielefeldt, A. Kirsch, O. Marti, J. Mlynek, and J. F. Marko, Europhys. Lett. **29**, 353 (1995); K. Tanaka, A. Takahara, and T. Kajiyama, Macromolecules **29**, 3232 (1996).
[14] L. V. Govor, G. Reiter, G. H. Bauer, and J. Parisi, Phys. Lett. A **353**, 198 (2006).
[15] A. W. Adamson, *Physical Chemistry of Surfaces* (Wiley, New

York, 1982).
[16] G. J. Hirasaki, J. Adhes. Sci. Technol. **7**, 285 (1993); T. J. Kneafsey and J. R. Hunt, J. Contam. Hydrol. **68**, 143 (2004).
[17] H. Dobbs and D. Bonn, Langmuir **17**, 4674 (2001).
[18] F. Brochard Wyart, P. Martin, and C. Redon, Langmuir **9**, 3682 (1993).
[19] C. Redon, F. Brochard-Wyart, and F. Rondelez, Phys. Rev. Lett. **66**, 715 (1991).
[20] P. G. de Gennes, Rev. Mod. Phys. **57**, 827 (1985).
[21] J. N. Israelachvili, *Intermolecular and Surface Forces* (Academic, London, 1991).
[22] F. Brochard-Wyart, P. G. de Gennes, H. Hervert, and C. Redon, Langmuir **10**, 1566 (1994); C. Redon, J. B. Brzoska, and F. Brochard-Wyart, Macromolecules **27**, 468 (1994); G. Reiter, P. Auroy, and L. Auvray, *ibid.* **29**, 2150 (1996); G. Reiter and R. Khanna, Phys. Rev. Lett. **85**, 2753 (2000).
[23] P. A. Kralchevsky, N. D. Denkov, V. N. Paunov, O. D. Velev, I. B. Ivanov, H. Yoshimora, and K. Nagayama, J. Phys.: Condens. Matter **6**, A395 (1994).
[24] E. Adachi, A. S. Dimitrov, and K. Nagayama, Langmuir **11**, 1057 (1995).
[25] R. D. Deegan, O. Bakajin, T. F. Dupont, G. Huber, S. R. Nagel, and T. A. Witten, Phys. Rev. E **62**, 756 (2000).
[26] H. C. Hamaker, Physica (Amsterdam) **9**, 1058 (1937).
[27] J. Visser, Adv. Colloid Interface Sci. **3**, 331 (1972).
[28] J. T. Davies and E. K. Rideal, *Interfacial Phenomenon* (Academic, New York, 1963).